

Non-uniform shrinkage in simply-supported composite steel-concrete slabs

Safat Al-Deen ^{1a}, Gianluca Ranzi ^{*2} and Brian Uy ^{3b}

¹ School of Engineering and Information Technology, UNSW Canberra
at the Australian Defence Force Academy, Canberra, Australia

² School of Civil Engineering, The University of Sydney, Sydney NSW 2006, Australia

³ Centre for Infrastructure Engineering & Safety, School of Civil and Environmental Engineering,
UNSW Australia, NSW 2052, Australia

(Received May 24, 2012, Revised July 02, 2013, Accepted June 11, 2014)

Abstract. This paper presents the results of four long-term experiments carried out to investigate the time-dependent behaviour of composite floor slabs with particular attention devoted to the development of non-uniform shrinkage through the slab thickness. This is produced by the presence of the steel deck which prevents moisture egress to occur from the underside of the slab. To observe the influence of different drying conditions on the development of shrinkage, the four 3.3 m long specimens consisted of two composite slabs cast on Stramit Condeck HP[®] steel deck and two reinforced concrete slabs, with the latter ones having both faces exposed for drying. During the long-term tests, the samples were maintained in a simply-supported configuration subjected to their own self-weight, creep and shrinkage for four months. Separate concrete samples were prepared and used to measure the development of shrinkage through the slab thickness over time for different drying conditions. A theoretical model was used to predict the time-dependent behaviour of the composite and reinforced concrete slabs. This approach was able to account for the occurrence of non-uniform shrinkage and comparisons between numerical results and experimental measurements showed good agreement. This work highlights the importance of considering the shrinkage gradient in predicting shrinkage deformations of composite slabs. Further comparisons with experimental results are required to properly validate the adequacy of the proposed approach for its use in routine design.

Keywords: composite; concrete; shrinkage; slabs; steel

1. Introduction

Composite steel-concrete slabs are a popular form of construction which consists of a solid slab cast on profiled steel sheeting. The advantage of this approach relies on the use of the steel deck as permanent formwork and, once the concrete hardens, as external reinforcement. Most research carried out to date has focussed on the ultimate response of composite slabs, e.g., (Porter and Ekberg Jr. 1977, Porter 1985, Stark and Brekelmans 1990, Daniels and Crisinel 1993, Veljković

*Corresponding author, Associate Professor, E-mail: gianluca.ranzi@sydney.edu.au

^a Lecturer, E-mail: s.al-deen@adfa.edu.au

^b Professor, E-mail: b.uy@unsw.edu.au

1998, Marimuthu *et al.* 2007, Lopes and Simões 2008, A-H Eldib *et al.* 2009, Kim and Jeong 2010), and on the identification of the interface properties between the concrete and the profiled sheeting, e.g., (Airumyan 1990, Patrick and Poh 1990, Patrick and Bridge 1994, Easterling and Young 1992, Veljkovic 1996, Crisinel and Marimon 2004, Jeong *et al.* 2005, Abdullah and Easterling 2009, Chen and Shi 2011, Chen *et al.* 2011, Seres and Dunai 2011). Very limited experimental work has been reported in the literature on the long-term behaviour of composite steel-concrete members, most of which dealing with traditional composite T-beams (e.g., Roll 1971, Johnson 1987, Alsamsam 1991, Bradford and Gilbert 1991, Wright *et al.* 1992, Uy 1997, Fan *et al.* 2010, Al-deen *et al.* 2011a, Al-Deen *et al.* 2012) and with only few studies focussing on the time-dependent response of composite slabs, e.g., (Al-deen *et al.* 2011b, Gilbert *et al.* 2012, Gholamhoseini *et al.* 2012). A comprehensive state of the art on the long-term behaviour of composite members can be found in (Ranzi *et al.* 2013b). The particularity of the long-term behaviour of composite floor systems relies on the development of a shrinkage gradient induced by the presence of the profiled sheeting which prevents moisture to egress from the underside of the slab, e.g., (Ranzi and Vrcelj 2009, Bradford 2010, Al-deen *et al.* 2011b, Gilbert *et al.* 2012; Gholamhoseini *et al.* 2012, Ranzi *et al.* 2013a). At present, structural engineers ignore the influence of this non-uniform shrinkage profile, because no design models or guidelines are currently available for this form of construction.

In this context, this paper presents new experimental data for the evaluation of the influence of the steel sheeting on the time-dependent response of composite slabs and for the benchmarking of analytical and numerical models. A theoretical model is then presented to describe the long-term behaviour of composite slabs extending previous work of the authors (Al-deen *et al.* 2011b, Gilbert and Ranzi 2011) to account for non-uniform shrinkage effects. This model is applied to predict the response of the four simply-supported slabs described in this study and its numerical results show good agreement with the experimental measurements. These comparisons highlight the need to account for the non-uniform shrinkage profile for an adequate prediction of the response of the composite simply-supported samples. Despite this, further work is required to be able to use the proposed approach for routine design.

2. Experimental programme

2.1 Overview

The aim of the experimental programme is to collect experimental data on the development of non-uniform shrinkage through the thickness of composite slabs. This non-uniform behaviour is induced by the presence of the steel deck which prevents moisture egress to occur from the underside of the slabs. For this purpose, four simply-supported slabs were prepared and monitored over four months subjected to their own self-weight, creep and shrinkage. In particular, this study included two composite slabs (with their underside sealed by the presence of the steel deck) and two reinforced concrete samples (with both slab faces exposed for drying) constructed with equivalent amounts of reinforcement to better highlight the role of the profiled sheeting on the development of the non-uniform shrinkage. Separate tests were carried out to obtain the instantaneous and long-term properties of the materials used in the experiments. Additional concrete samples were prepared and monitored over time to experimentally measure the development of the non-uniform shrinkage when a slab is sealed on one surface and exposed for drying on its opposite one, such as it occurs in the presence of the steel deck.

2.2 Simply-supported composite and reinforced concrete slabs

Four simply-supported slabs were prepared and monitored over time subjected to their own self-weight, creep and shrinkage effects. All samples had a total length of 3.3 m, with a distance between roller supports of 3.0 m.

Two specimens, referred to as CS1 and CS2, consisted of two composite slabs cast on 0.75 mm Stramit Condeck HP[®] profiled sheeting (Fig. 1) and differed in the amount of reinforcement. This steel deck profile possesses an area and a second moment of area (per meter width of steel sheeting) equal to 1211 mm² and 488×103 mm⁴, respectively (Stramit 2012). Sample CS1 was prepared with no reinforcing bars, while five N16 reinforcing bars (Onesteel 2012) were used for CS2 (Figs. 2(a) and (b)). The number of bars was selected to specify equivalent areas of reinforcement in the top and bottom of the section. With the proposed arrangement the steel deck area of 1090 mm² (based on the 900 mm sample slab width), i.e., representing the bottom layer of reinforcement, was balanced with the 1000 mm² nominal area of the top N16 reinforcing bars. The exact location of the reinforcement is reported in Section 4.

The remaining two samples were reinforced concrete slabs, which were denoted as SS1 and SS2. The samples were able to dry from both top and bottom surfaces, unlike the composite

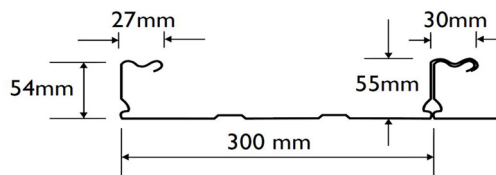
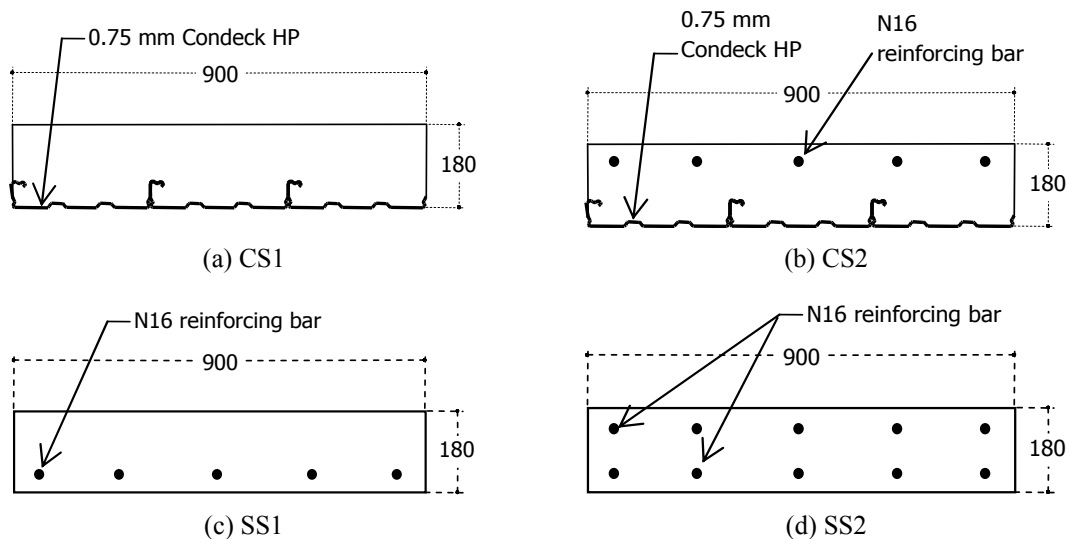


Fig. 1 Details of the 0.75 mm Condeck HP steel deck profile



*Note: refer to section 4 for the exact location of the reinforcement

Fig. 2 Details of the cross-section of simply-supported slabs

specimens which could dry only from their top face. Also in this case, two arrangements were used for the reinforcement as illustrated in Figs. 2(c) and (d). In this manner, the amounts of reinforcement specified for samples SS1 and SS2 were equivalent to those adopted for CS1 and CS2, respectively, while differing for the drying conditions related to the underside of the slab and consequent shrinkage profiles.

All specimens were cast at the same time under propped conditions with the same batch of concrete. The specimens were moist cured for 15 days from concrete pouring. On day 15 the props were removed and the samples were placed under simply-supported conditions subjected to their own self-weight, creep and shrinkage affects. Layout of the long-term arrangement is outlined in Fig. 3. The variations in slab deflections were continuously monitored by means of LVDTs and strain gauges placed at the mid-span of each sample. In particular, strain gauges were placed at the top and bottom surfaces of the slab while embedded strain gauges were inserted at third points through the slab thickness as shown in Fig. 4. Before the concrete pour, each embedded strain gauge was suspended in its position using two very thin fishing wires running perpendicular to the direction of the strain measurement. The wires were anchored to the formwork and were carefully tensioned. The two ends of the strain gauge were supported on the two parallel wires, tied to them with a thin thread and firmly positioned by the addition of a drop of glue. Special care was taken during concrete pouring to minimise the movement of the embedded strain gauges. All LVDTs and strain gauges were connected to dataloggers which recorded data every 2 hours for the entire duration of the experiment.

The long-term mid-span deflections recorded for the four slabs are shown in Fig. 5. These do not include the instantaneous components of the deflections taken place after the removal of the props and consider only the long-term deformations due to creep and shrinkage. From these

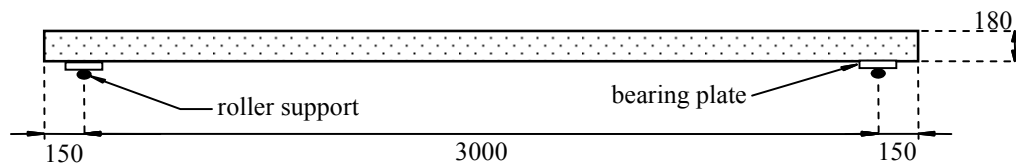


Fig. 3 Set-up of the long-term experiments for the simply-supported slabs

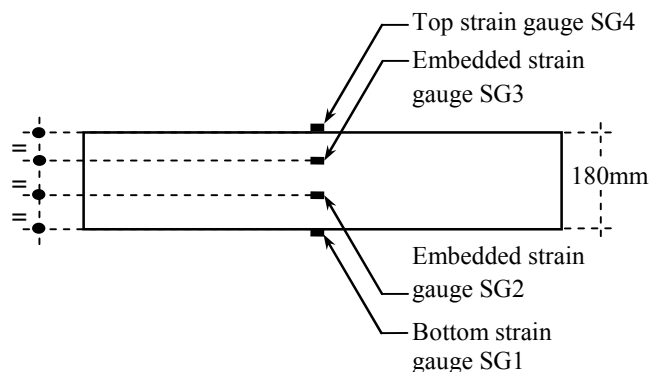


Fig. 4 Location of strain measurements at mid-span section of the simply-supported slabs and of the shrinkage slab samples

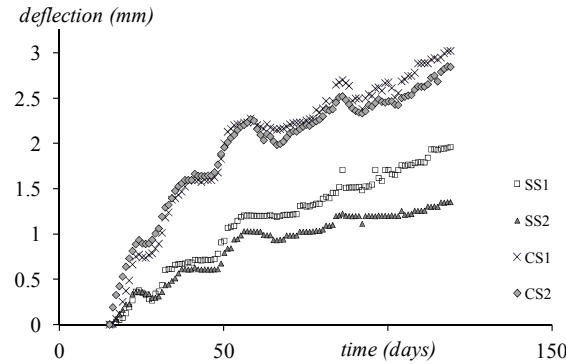


Fig. 5 Long-term mid-span deflections of the simply-supported slabs

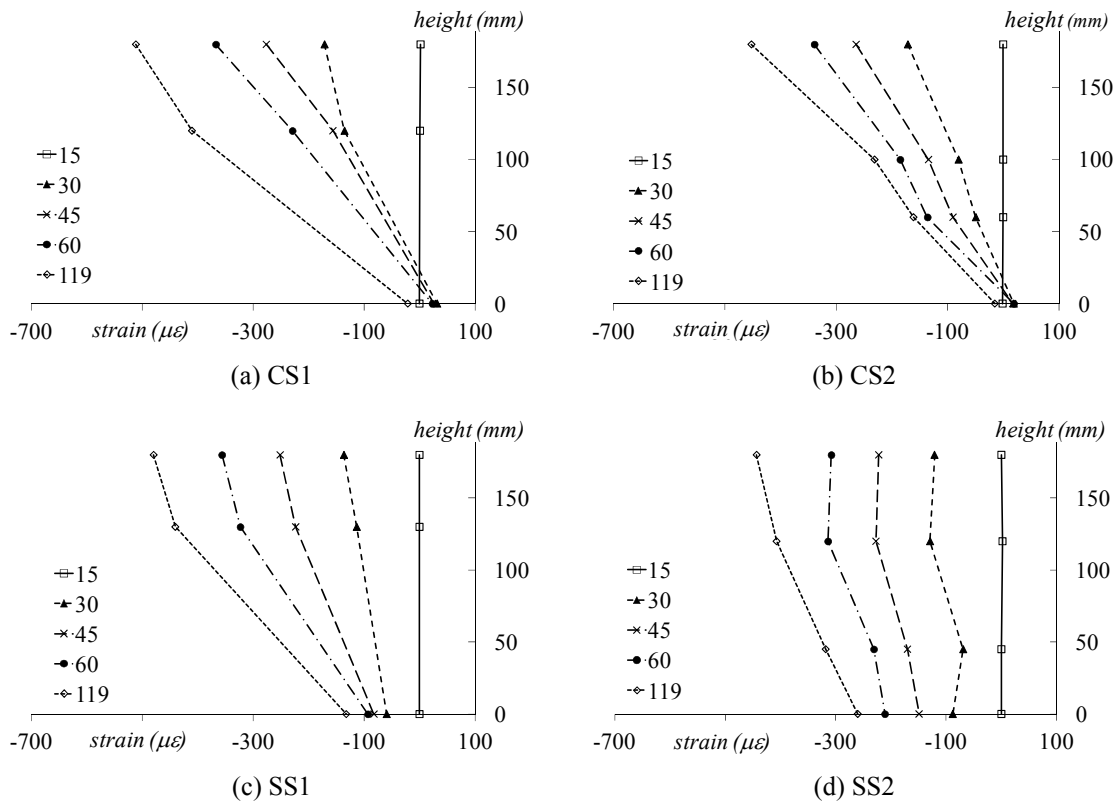


Fig. 6 Long-term strain readings measured at mid-span section of the simply-supported slabs

measurements, it can be observed that the deflections undergone by the composite slabs were greater than those observed for the reinforced concrete slabs. For example, the deflections of CS1 and SS1 after 119 days from casting were 3.02 mm and 1.96 mm, respectively, despite having similar amounts of steel reinforcement (either in the form of bars or sheeting). The greater displacement of CS1, i.e., 54% larger, was attributed to the non-uniform shrinkage profile

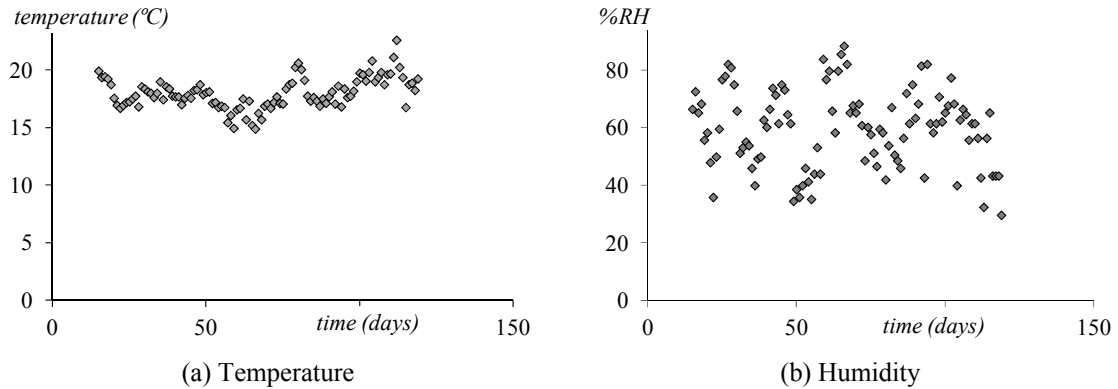


Fig. 7 Average ambient temperature and humidity

developed in CS1. Similar considerations were carried out for samples CS2 and SS2 with deflections of 2.85 mm and 1.35 mm, respectively. In this case, the composite value after 119 days was 110% greater than the one of the solid slab. These differences were confirmed by other recent studies carried out on composite and post-tensioned composite slabs. (Al-deen *et al.* 2011b, Gilbert *et al.* 2012, Gholamhoseini *et al.* 2012, Ranzi *et al.* 2013a).

Strain measurements recorded through the slab thickness at different points in times are presented in Fig. 6. These readings represent only the long-term deformations taking place after the removal of the props. From Fig. 6 it can be noted that bottom strain values measured for the composite slabs tend to remain close to zero with curvatures growing over time. This was not the case for the solid samples which exhibited a more uniform total strain distribution through the slab thickness. These differences were attributed to the different shrinkage profiles being developed in the two types of samples.

Ambient temperature and humidity were recorded for the entire duration of the long-term tests and average values are reported in Fig. 7.

2.3 Samples monitoring the development of non-uniform shrinkage

Three specimens were prepared to monitor the development of total deformations induced by shrinkage effects through the slab thickness of solid and composite slabs and, because of this, are referred to as shrinkage slabs in the following. These were cast unreinforced and kept unloaded to monitor shrinkage effects only. In reality, these samples were also subjected to creep produced by their self-weight, even if the magnitude of these deformations is negligible (at least for the samples considered) when compared to the strains exhibited due to shrinkage. The dimensions of the shrinkage slabs were 900 mm × 900 mm, with a thickness of 180 mm. These were prepared with the same batch of concrete and curing conditions used for the simply-supported slabs. The differences between the three shrinkage slabs, denoted as SH1, SH2 and SH3, related to their boundary conditions and to the presence of the steel deck as detailed in Table 1. In particular, specimen SH1 consisted of a solid slab with both top and bottom faces exposed to the environment, so that drying could occur from both faces. Specimen SH2 was identical to SH1 with the only difference that the bottom face of the slab was sealed by means of a plastic sheet. This setup represented the sealed condition provided by the steel deck without inducing its restraining action.

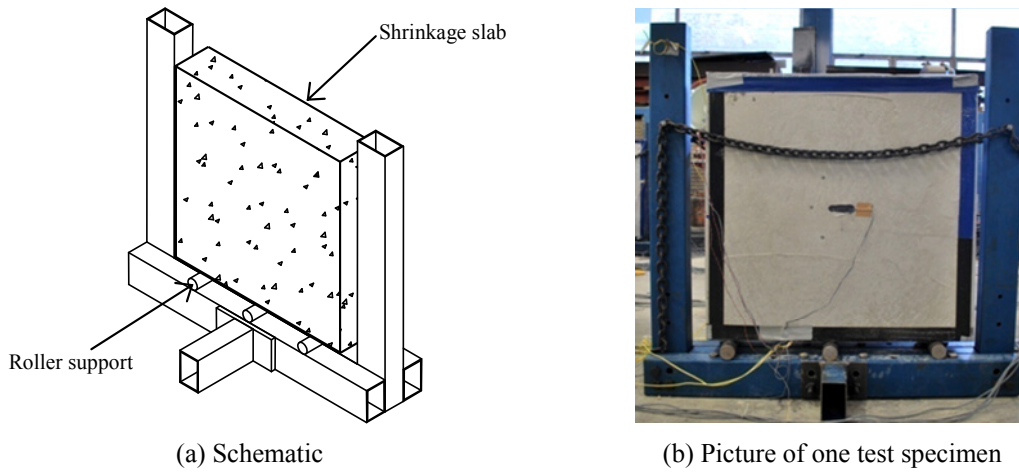


Fig. 8 Test layout for the long-term measurements carried out for samples SH1, SH2 and SH3

Table 1 Details of shrinkage slab samples

Shrinkage sample ID	Dimensions of samples			Exposed conditions of top and bottom surfaces
	(mm)	(mm)	(mm)	
SH1	900	900	180	Top and bottom exposed
SH2	900	900	180	Top exposed Bottom sealed with plastic
SH3	900	900	180	Top exposed Bottom sealed with Condeck HP

*NOTE: all slab edges are sealed with plastic

Specimen SH3 was cast on Condeck HP in which case the steel deck prevented moisture egress to take place from the underside of the slab and provided an eccentric restraint to the slab. All side edges were sealed with plastic to prevent drying to take place from these locations as it would occur in a real slab due to its continuity. During the long-term measurements samples SH1-SH3 were placed vertically on three roller supports as outlined in Fig. 8. This arrangement enabled the specimens to deform freely without any external restraint provided by the supporting frame.

Long-term deformations were measured using surface and embedded strain gauges placed through the thickness of the slabs based on the arrangement already depicted in Fig. 4 for SS1, SS2, CS1 and CS2. Strain gauges were installed to measure horizontal deformations, to minimise the possible influence of the self-weight on the readings. The strain variations observed over time for samples SH1-SH3 are shown in Fig. 9. Representative strain profiles measured through the thickness of the shrinkage slabs at different instants in time are presented in Fig. 10. These readings highlight the fact that strains exhibit an uniform profile through the slab thickness when the sample is free to dry from both top and bottom surfaces, as for SH1. Significant strain gradients developed over time for SH2 due to the sealed condition provided by the plastic placed on the underside of the slab. Specimen SH3 showed the development of a gradient as well, although these measurements were also influenced by the retraining action provided by the

presence of the profiled sheeting.

Even if shrinkage distributions possess non-uniform profiles through the thickness of a slab (Gilbert and Ranzi 2011), it is common to assume a linear profile for its representation in design. Under this condition, the total deformations plotted in Figs. 9(a)-(b) and 10(a)-(b) can be assumed to directly reflect the shrinkage distributions of a solid slab and a composite one, respectively. For example, the results for SH1 outline a constant shrinkage profile confirming the adequacy of such assumption commonly adopted in the design of solid slabs. Similarly, the strain profile recorded for SH2 depicts the shrinkage distribution to be used for a composite slab, when drying takes place from one side of the slab only.

2.4 Material properties

2.4.1 Instantaneous concrete properties

Two sets of standard concrete cylinders (with height of 300 mm and diameter of 150 mm) were tested to determine the concrete strength at 15 and 28 days from the concrete pour, with measured average compressive strengths of 18.3 MPa and 27.3 MPa, respectively. An elastic modulus of 19,000 MPa was measured at 15 days from concrete casting.

2.4.2 Concrete shrinkage

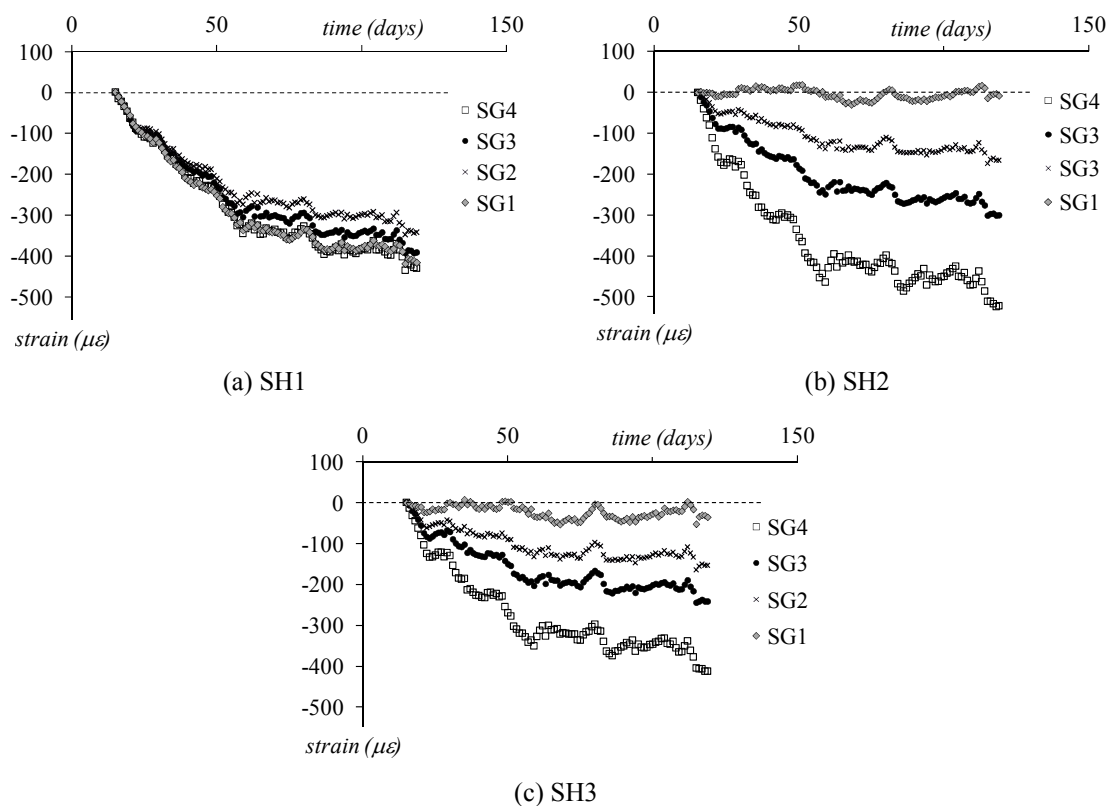


Fig. 9 Total deformations measured at different levels of the cross-sections for samples SH1, SH2 and SH3

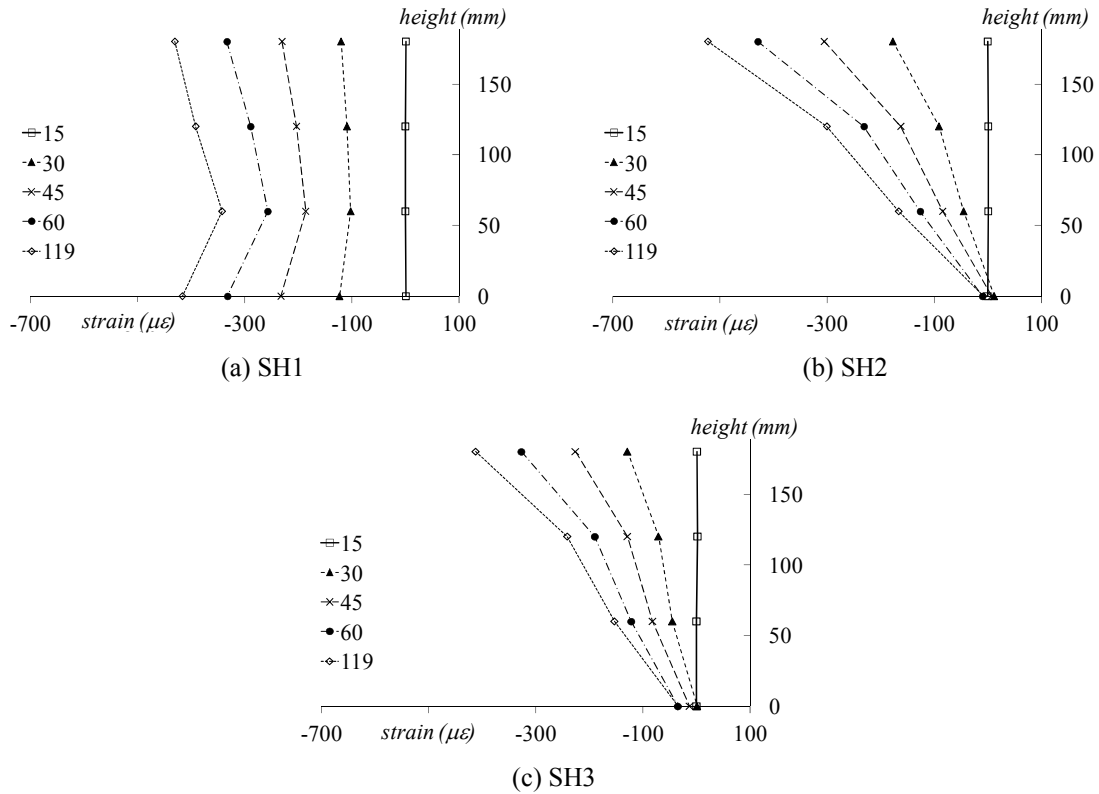


Fig. 10 Total long-term deformation measured through the thickness of SH1, SH2 and SH3

Free shrinkage of the concrete was observed recording the deformations of two concrete cylinders (with diameter 150 mm and height 300 mm). Shrinkage measurements started after 15 days from casting, day at which the curing of all concrete samples was terminated. Fig. 11(a) shows the average shrinkage strains measured from the two cylinders over time.

2.4.3 Concrete creep

Three standard concrete cylinders (with diameter 150 mm and height 300 mm) were used to measure the occurrence of creep. They were loaded at 15 days from casting with a sustained load producing a stress of 5.75 MPa. Total deformations measured for these samples over time are reported in Fig. 11(b). The corresponding creep coefficients $\varphi(t,15)$ calculated at a generic instant in time t (for the sustained load applied at 15 days after casting) were calculated from the total strain and shrinkage readings as follows

$$\varphi(t,15) = \frac{\varepsilon_{cr}}{\varepsilon_i} = \frac{\varepsilon_{tot}}{\varepsilon_i} - \frac{\varepsilon_{sh}}{\varepsilon_i} - 1 \tag{1}$$

where ε_{tot} is the total strain (Fig. 11(b)), ε_i represents the instantaneous strain, ε_{cr} is the creep strain, and the shrinkage strain is denoted by ε_{sh} (Fig. 11(a)). The calculated creep coefficients are plotted in Fig. 11(c).

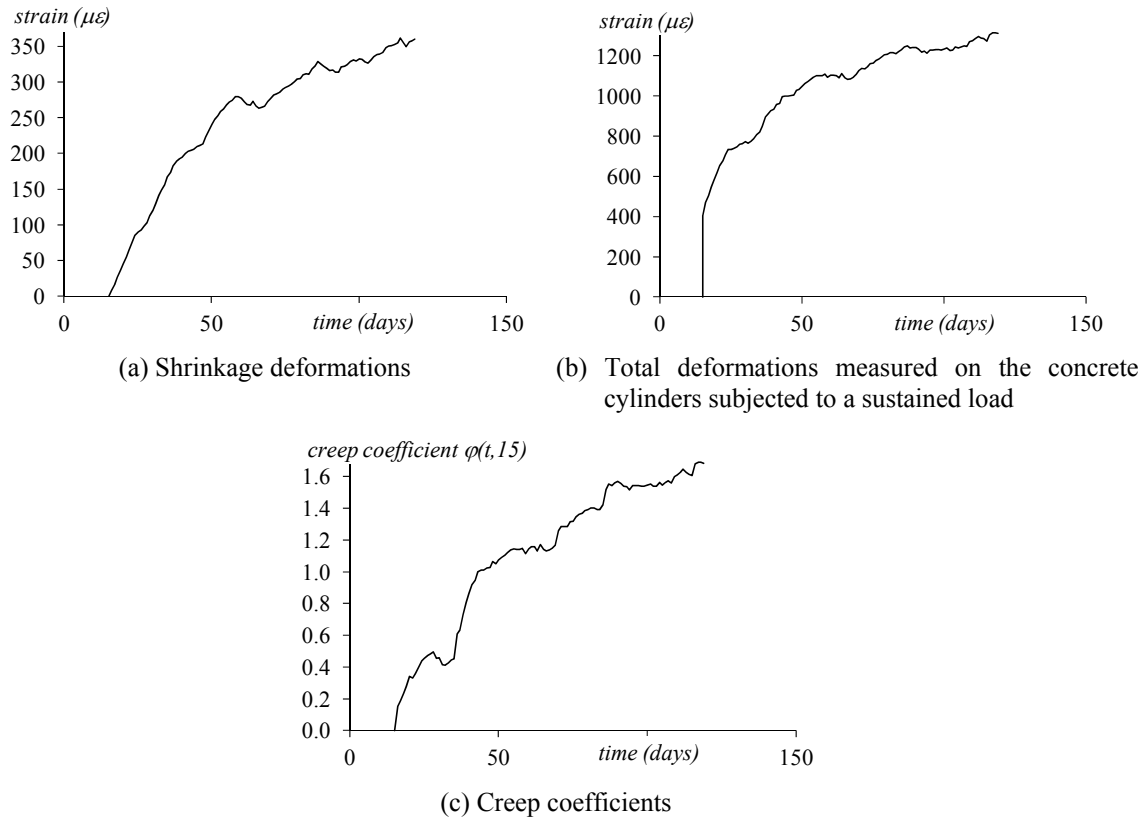


Fig. 11 Time-dependent properties of the concrete

2.4.4 Steel sheeting and reinforcing bar

The properties of the steel sheeting and reinforcing bars were obtained from standard tensile tests. Yield and ultimate strengths were 601.4 MPa and 629.3 MPa, respectively, for the Condeck HP profile, while measurements for the reinforcing bar were 598.5 MPa and 661.3 MPa, respectively.

3. Theoretical modelling

3.1 Assumptions

An analytical model was derived to describe the short- and long-term behaviour of the simply-supported slabs. This was able to account for the occurrence of non-uniform shrinkage, observed to occur in composite slabs. The proposed formulation is based on the assumptions of Euler-Bernoulli beam theory, in which plane sections remain plane and perpendicular to the beam axis before and after deformations. It is also assumed that there is no slip at the interface between steel sheeting and concrete slab. A cross-sectional analysis procedure was used to determine the variation of deformations taking place over time at different locations along the slab length, based

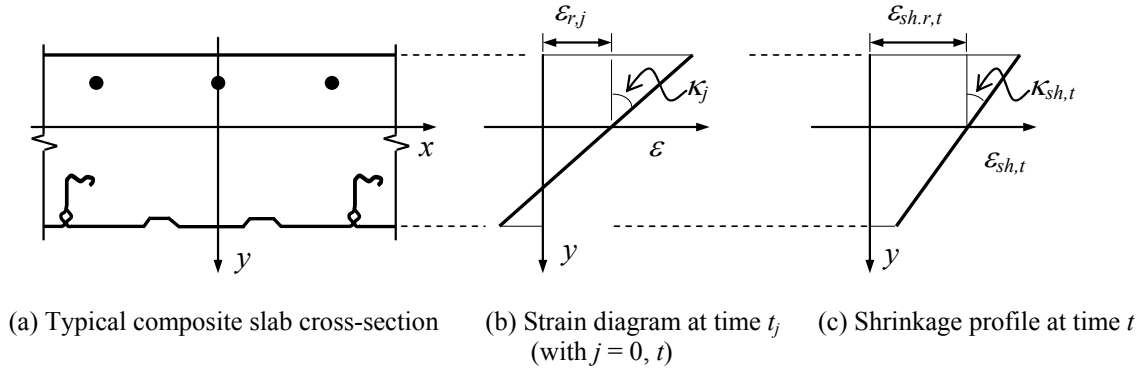


Fig. 12 Generic cross-section and strain profiles considered in the numerical model

on which the member response was evaluated.

The composite cross-section considered in the model presented below is formed by a concrete component, reinforcing bars and a steel deck, as shown in Fig. 12. The case of a reinforced concrete slab can be easily considered by eliminating the terms related to the profiled sheeting from the model.

3.2 Material properties

The steel sheeting and the steel reinforcements are assumed to behave in a linear-elastic fashion, with E_d and E_s being the elastic moduli for the deck and reinforcing bars, respectively. This is commonly acceptable for numerical calculations carried out at service conditions. (Gilbert and Ranzi 2011).

The behaviour of the concrete is assumed to be time-dependent, and it is modelled using the Age-adjusted Effective Modulus Method (AEMM) (Bazant 1972). It is also assumed that its time-dependent response is identical in both compression and tension, as recommended in Gilbert and Ranzi (2011) and Bazant and Oh (1984) for stress levels in compression (tension) less than about one half of the compressive (tensile) strength of the concrete. The long-term behaviour of the concrete is then defined at time t_0 (where t_0 depicts the time of first loading) and at a generic instant in time t as: (Bazant 1972, CEB 1984, Gilbert and Ranzi 2011).

$$\sigma_{c,0} = E_{c,0} \varepsilon_{c,0} \tag{2a}$$

$$\sigma_{c,t} = \bar{E}_{e,t} (\varepsilon_{c,t} - \varepsilon_{sh,t}) + \sigma_{c,0} \bar{F}_{e,0} \tag{2b}$$

and

$$\bar{E}_{e,t} = \frac{E_{c,0}}{1 + \chi(t, t_0) \varphi(t, t_0)} \tag{3a}$$

$$\bar{F}_{e,0} = \frac{\varphi(t, t_0) [\chi(t, t_0) - 1]}{1 + \chi(t, t_0) \varphi(t, t_0)} \tag{3b}$$

where subscripts ‘0’ and ‘ t ’ are used to distinguish between variables calculated at times t_0 and t , σ_c and ε_c represent the concrete stress and total strain, $E_{c,0}$ and $\bar{E}_{e,t}$ depict the elastic modulus of concrete calculated at t_0 and the age-adjusted effective modulus, $\bar{F}_{e,0}$ is the age-adjusted creep factor, while $\varphi(t, t_0)$ and $\chi(t, t_0)$ define the creep and aging coefficients, respectively. For the purpose of this paper, the values adopted for the aging coefficients in the numerical calculations have been approximated by 0.65 and 0.8, which fall within the range of commonly used values. (Gilbert and Ranzi 2011, CEB 1984).

3.3 Instantaneous cross-sectional analysis

The governing system of equations describing the cross-sectional analysis at time t_0 is expressed in terms of two unknowns defining the strain diagram, which consist of the strain measured at the level of the reference axis $\varepsilon_{r,0}$ and of the curvature κ_0 (Fig. 12(b)). These are then determined enforcing equilibrium considerations at the cross-section as outlined below.

The internal axial force $N_{int,0}$ and moment $M_{int,0}$ resisted at t_0 by the cross-section can be expressed as

$$N_{int,0} = R_{A,0} \varepsilon_{r,0} + R_{B,0} \kappa_0 \quad (4a)$$

$$M_{int,0} = R_{B,0} \varepsilon_{r,0} + R_{I,0} \kappa_0 \quad (4b)$$

in which $R_{A,0}$, $R_{B,0}$ and $R_{I,0}$ define the axial rigidity, the stiffness related to the first moment of area and the flexural rigidity, respectively. These are determined based on

$$R_{A,0} = A_c E_{c,0} + A_d E_d + \sum_{i=1}^{m_s} A_{s(i)} E_{s(i)} \quad (5a)$$

$$R_{B,0} = B_c E_{c,0} + B_d E_d + \sum_{i=1}^{m_s} y_{s(i)} A_{s(i)} E_{s(i)} \quad (5b)$$

$$R_{I,0} = I_c E_{c,0} + I_d E_d + \sum_{i=1}^{m_s} y_{s(i)}^2 A_{s(i)} E_{s(i)} \quad (5c)$$

where the area, first and second moments of area of the concrete are denoted with A_c , B_c and I_c , respectively. In a similar way, the geometric properties for the steel deck are referred to with A_d , B_d and I_d . With the adopted notation, the reinforcing bars located at the same level of the cross-section are assumed to be lumped together, with $y_{s(i)}$ and $A_{s(i)}$ depicting the position and area of the i -th layer of reinforcement (with $i = 1, \dots, m_s$).

The unknown strain variables can then be evaluated applying force and moment equilibrium at the cross-section between internal and external actions

$$N_{int,0} = N_{e,0} \quad (6a)$$

$$M_{int,0} = M_{e,0} \quad (6b)$$

where $N_{e,0}$ and $M_{e,0}$ represent the external axial force and moment, respectively. Eq. (6) can then be

solved to obtain the expressions for $\varepsilon_{r,0}$ and κ_0 as follows

$$\varepsilon_{r,0} = \frac{R_{I,0}N_{e,0} - R_{B,0}M_{e,0}}{R_{A,0}R_{I,0} - R_{B,0}^2} \quad (7a)$$

$$\kappa_0 = \frac{R_{A,0}M_{e,0} - R_{B,0}N_{e,0}}{R_{A,0}R_{I,0} - R_{B,0}^2} \quad (7b)$$

which define the strain diagram at time t_0 and from which the stress distributions can be calculated recalling the adopted material properties.

The proposed approach can be easily modified to account for concrete cracking as, for example, presented in (Gilbert and Ranzi 2011) when dealing with concrete members subjected to external loads, creep and uniform shrinkage.

3.4 Long-term cross-section analysis

Similarly to the instantaneous case, the system of equations governing the structural behaviour at a generic instant in time t is expressed as a function of the variables describing the strain diagram as unknowns. In particular, the selected parameters consist of the strain measured at the level of the reference axis $\varepsilon_{r,t}$ and of the curvature κ_t (Fig. 12(b)). For clarity, the subscript ‘ t ’ is adopted for variables calculated at the generic instant in time t , to distinguish them from their corresponding values obtained at t_0 , for which the adopted subscript was ‘0’.

The strain variables are then determined enforcing equilibrium at the cross-sections between internal and external axial forces, referred to as $N_{int,t}$ and $N_{e,t}$, and internal and external moments, denoted as $M_{int,t}$ and $M_{e,t}$, which can be written as

$$N_{int,k} = N_{e,k} \quad (8a)$$

$$M_{int,k} = M_{e,k} \quad (8b)$$

Based on the adopted material properties, $N_{int,t}$ and $M_{int,t}$ can be expressed as

$$N_{int,t} = R_{A,t}\varepsilon_{r,t} + R_{B,t}\kappa_t + \bar{F}_{e,0}N_{c,0} - R_{Ac,t}\varepsilon_{sh,r,t} - R_{Bc,t}\kappa_{sh,t} \quad (9a)$$

$$M_{int,t} = R_{B,t}\varepsilon_{r,t} + R_{I,t}\kappa_t + \bar{F}_{e,0}M_{c,0} - R_{Bc,t}\varepsilon_{sh,r,t} - R_{Ic,t}\kappa_{sh,t} \quad (9b)$$

where $N_{c,0}$ and $M_{c,0}$ are the axial force and moment resisted by the concrete at time t_0 , and variables $\varepsilon_{sh,r,t}$ and $\kappa_{sh,t}$ define the shrinkage profile applied to the cross-section at the time considered based on the linear distribution depicted in Fig. 12(c). Their values are assumed to be known because defined based on the material properties of the concrete. In this way, the shrinkage values at a particular level of the cross-section can be calculated from

$$\varepsilon_{sh,t} = \varepsilon_{sh,r,t} + y\kappa_{sh,t} \quad (10)$$

The rigidities of the composite cross-section at time t are determined based on

$$R_{A,t} = A_c \bar{E}_{e,t} + A_d E_d + \sum_{i=1}^{m_s} A_{s(i)} E_{s(i)} \quad (11a)$$

$$R_{B,t} = B_c \bar{E}_{e,t} + B_d E_d + \sum_{i=1}^{m_s} y_{s(i)} A_{s(i)} E_{s(i)} \quad (11b)$$

$$R_{I,t} = I_c \bar{E}_{e,t} + I_d E_d + \sum_{i=1}^{m_s} y_{s(i)}^2 A_{s(i)} E_{s(i)} \quad (11c)$$

while the concrete properties are obtained using

$$R_{Ac,t} = A_c \bar{E}_{e,t} \quad (11d)$$

$$R_{bc,t} = B_c \bar{E}_{e,t} \quad (11e)$$

$$R_{Ic,t} = I_c \bar{E}_{e,t} \quad (11f)$$

The system of equations required to solve for the unknown $\varepsilon_{r,t}$ and κ_t can be obtained substituting Eq. (9) into Eq. (8), from which their expressions can be written as

$$\varepsilon_{r,t} = \frac{R_{I,t}(N_{e,t} - \bar{F}_{e,o} N_{c,0} + R_{Ac,t} \varepsilon_{sh,r,t} + R_{Bc,t} \kappa_{sh,t}) - R_{B,t}(M_{e,t} - \bar{F}_{e,o} M_{c,0} + R_{Bc,t} \varepsilon_{sh,r,t} + R_{Ic,t} \kappa_{sh,t})}{R_{I,t} R_{I,t} - R_{B,t}^2} \quad (12a)$$

$$\kappa_t = \frac{R_{A,t}(M_{e,t} - \bar{F}_{e,o} M_{c,0} + R_{Bc,t} \varepsilon_{sh,r,t} + R_{Ic,t} \kappa_{sh,t}) - R_{B,t}(N_{e,t} - \bar{F}_{e,o} N_{c,0} + R_{Ac,t} \varepsilon_{sh,r,t} + R_{Bc,t} \kappa_{sh,t})}{R_{A,t} R_{I,t} - R_{B,t}^2} \quad (12b)$$

Once the values for the strain at the level of the reference axis $\varepsilon_{r,t}$ and curvature κ_t are determined, the solution at time t can be post-processed to obtain the relevant strain and stress distributions over the cross-section.

3.5 Short- and long-term member analysis

The member analysis at times t_0 and t is performed considering the deflected shape to vary along the member with a shape described by a fourth order polynomial. Based on this assumption, the mid-span deflections are determined based on the curvature values calculated at mid-span and at the ends of the slab: (Gilbert and Ranzi 2011)

$$v_j = \frac{L^2}{96} (\kappa_{(z=0),j} + 10\kappa_{(z=L/2),j} + \kappa_{(z=L),j}) \quad (13)$$

where the subscript ' j ' equals '0' for the instantaneous analysis and ' t ' for the long-term one, v_j

represents the mid-span vertical deflection of the slab at time t_j , L depicts the span of the slab, z is the coordinate along the member length, while $\kappa_{(z=0)_j}$, $\kappa_{(z=L/2)_j}$ and $\kappa_{(z=L)_j}$ define the curvature values calculated at time t_j from the cross-sectional calculations at the two ends and at mid-span of the slab.

4. Comparisons between numerical and experimental results

The method of analysis previously proposed is used in this section to predict the long-term behaviour of the simply-supported slabs reported in this study. Considering the fact that no cracking was observed in the slabs for the duration of the long-term experiments, the cross-sectional properties of the concrete have been based on its uncracked conditions.

The shrinkage profiles adopted in the calculations are those measured experimentally with samples SH1 (for the constant distribution representative of the case of a slab exposed on both

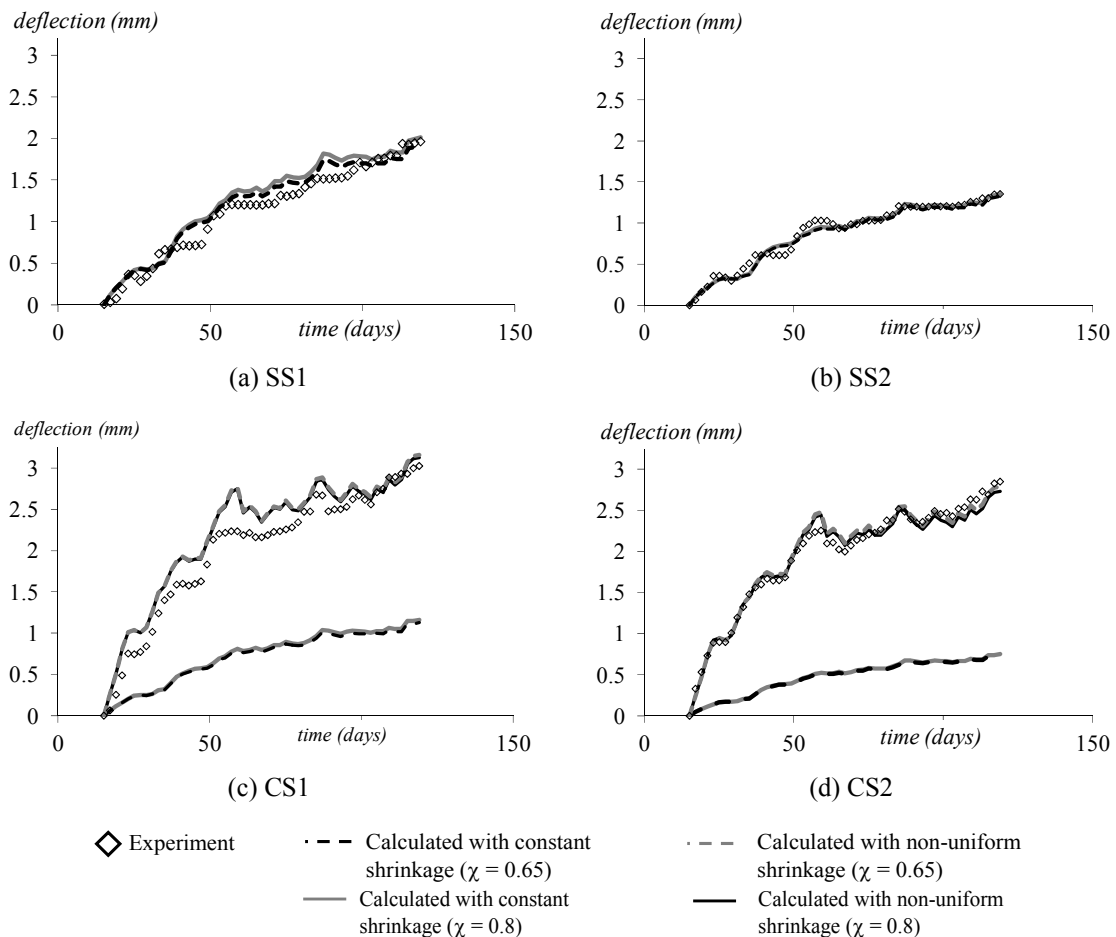


Fig. 13 Comparisons between experimental measurements and calculated values for the mid-span deflections

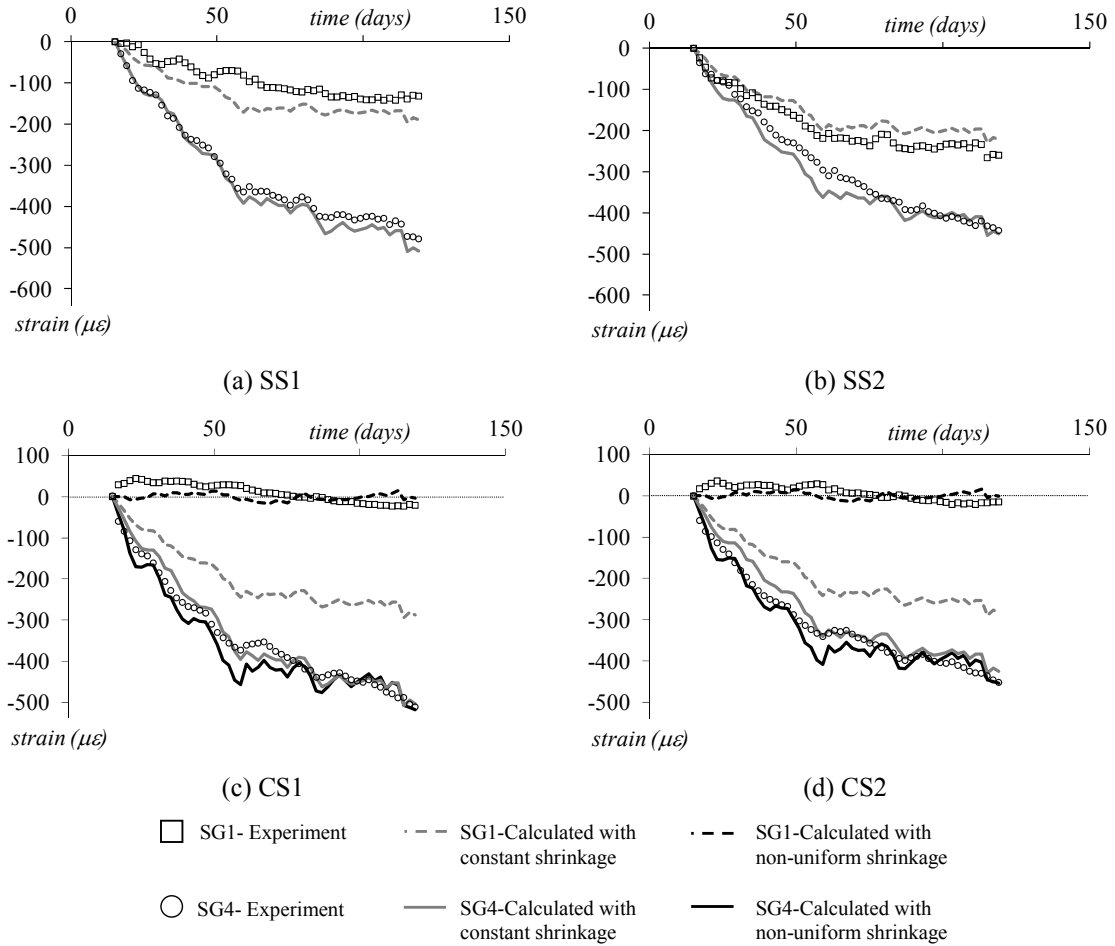


Fig. 14 Comparisons between numerical measurements and calculated values for the top and bottom slab strains

sides shown in Fig. 10(a)), and SH2 (to depict the non-uniform profile developing in a slab sealed on one side depicted in Fig. 10(b)). These considerations are based on the assumptions that the shrinkage distribution is linear, which is acceptable considering that the proposed approach intends to be suitable for design purposes.

The results presented for the mid-span deflections determined for the solid slabs SS1 and SS2 are based on the shrinkage profiles measured for SH1, which describe similar shrinkage readings as those measured from the concrete cylinders in Section 2.4.3. For the composite slabs CS1 and CS2, two sets of calculations have been carried out, one using the constant shrinkage of SH1 and the other based on the non-uniform shrinkage profile of SH2. For the creep coefficients, the values provided in Fig. 11(c) have been used in the calculations for the solid slabs SS1 and SS2 (this is acceptable considering that, in the case of the shrinkage strains, similar measurements were taken from slabs SH1 and the concrete cylinders). For the composite slabs CS1 and CS2, the creep coefficients adopted in the calculations have been approximated scaling the values plotted in Fig. 11(c) by a factor $k_{\phi,CS}$ to account for the sealed condition of the underside of the slab. In particular,

the value for $k_{\phi,CS}$ represents the ratio between the creep coefficients produced with the hypothetical thickness of the composite slab (equal to twice the slab thickness, to account for the sealed conditions of its underside) and those calculated with the hypothetical thickness of the solid slab (equal to the slab thickness), evaluated based on Australian guidelines (AS3600 2009).

Comparisons between the numerical results and the experimental measurements of the mid-span deflections are presented in Fig. 13. These have been calculated based on the material properties observed from the material tests presented in Section 2 and on the locations of the reinforcing bars determined from cutting the samples at the completion of the tests. In particular, it was found that the centroids of top reinforcement in SS2 and CS2 were located at 118 mm and 121 mm from the bottom of the slab, respectively, while the bottom bars for SS1 and SS2 were placed at 18 mm and 15 mm from the underside of the slab, respectively. The plotted results do not significantly depend, for the particular slab arrangements considered in this study, on the values adopted for the aging coefficients (i.e., 0.65 and 0.8). Because of this, following results are only reported, for clarity, based on an aging coefficient of 0.65. (Gilbert and Ranzi 2011).

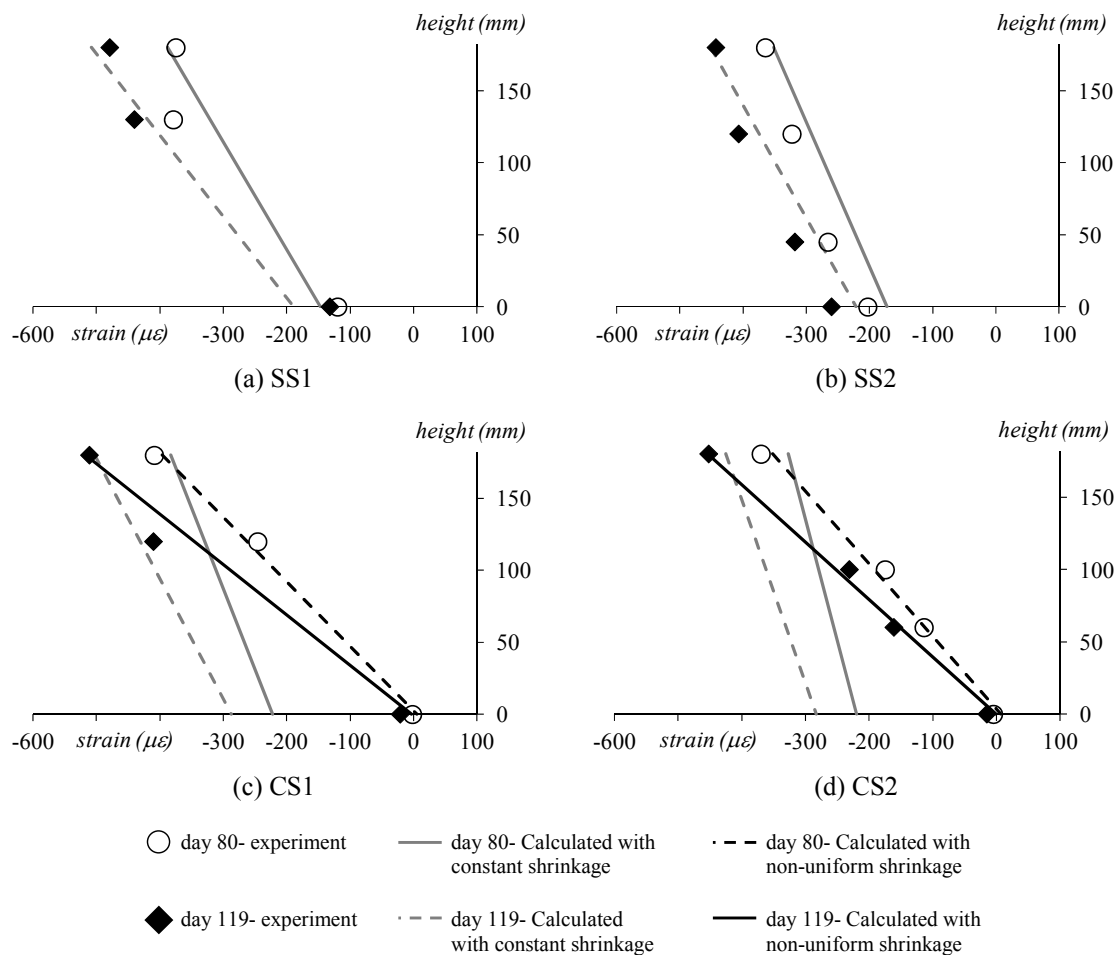


Fig. 15 Comparisons between experimental measurements and calculated values for the long-term mid-span strains at different instances in time

For the case of the solid slabs, a good match is obtained between numerical and experimental results (Figs. 13(a) and (b)) highlighting the adequacy of using the constant shrinkage profile for the predictions of the response of the solid slabs exposed on both sides.

In the case of composite slabs, the calculations have been carried out using both constant and non-uniform shrinkage distributions, as shown in Figs. 13(c) and (d). These results outline how the use of the constant profile can underestimate the predictions of the shrinkage deflections (Fig. 13(c)), which require the use of the non-uniform profile for an adequate representation (Fig. 13(d)). Similar trends were observed in other recent studies carried out on composite and post-tensioned composite slabs. (Al-deen *et al.* 2011b, Gilbert *et al.* 2012, Gholamhoseini *et al.* 2012, Ranzi *et al.* 2013a).

Comparisons between calculated and measured long-term strains are provided in Fig. 14, with cross-sectional distributions outlined in Fig. 15. Also in these cases, good agreement between experimental and numerical results is obtained for both solid and composite slabs, when considering for the latter the non-uniform shrinkage distribution. For samples CS1 and CS2, the top strain is reasonably well predicted with both constant and non-uniform shrinkage profiles, while the bottom deformation is overestimated with the constant shrinkage distribution. This implies that the latter representation underestimates also the curvature which develops in the member due to shrinkage, leading to underestimations of the deflections. Based on the measurements of these tests, it can be concluded that the non-uniform shrinkage profile needs to be considered in the analysis to obtain accurate strain values when dealing with composite slabs. Despite this, it should be noted that further validation of the model is required before adopting the proposed method of analysis for routine design.

5. Conclusions

This paper presented an experimental and numerical study on the time-dependent behaviour of composite slabs and on the occurrence of the non-uniform shrinkage distributions through their thickness. The latter is induced by the presence of the profiled sheeting which prevents moisture to egress from the underside of the slab. For this purpose, four samples were prepared, which consisted of two composite slabs poured on Condeck HP profiles (with their undersides sealed by the steel deck and top surface exposed for drying) and two reinforced concrete ones (with both top and bottom surfaces of the slabs exposed for drying). The two sets of samples, i.e., the composite and the reinforced concrete ones, contained equivalent reinforcement arrangements to monitor the development and effects of shrinkage based on the different exposures of the bottom of the slab. During the long-term tests, the four slabs were maintained in a simply-supported static configuration subjected to creep and shrinkage effects. It was observed that the non-uniform shrinkage profile of the composite specimens induced larger deflections than the reinforced concrete companion samples. The development of non-uniform shrinkage was monitored on separate concrete samples prepared with different exposure conditions, and separate tests were carried out to obtain instantaneous and time-dependent properties of the materials used in this study. A theoretical model was presented to predict the long-term response of composite slabs, able to account for the occurrence of non-uniform shrinkage distributions. The comparisons between numerical results and experimental measurements highlighted the importance of including the shrinkage gradient for an accurate prediction of the long-term deflections in composite slabs, and confirmed the adequacy of adopting a constant shrinkage profile for solid

slabs exposed on both sides. Further work is required to validate the adequacy of the proposed method of analysis for its use in routine.

Acknowledgments

The work in this article was supported under Australian Research Council's Linkage Projects funding scheme (project number LP0990190) and by Stramit Building Products and Arup as Partner Organisations. The experimental work was carried in the J.W. Roderick Materials and Structures Testing Laboratory of the School of Civil Engineering at the University of Sydney. The assistance of the laboratory staff is also acknowledged.

References

- A-H Eldib, M.E., Maaly, H.M., Beshay, A.W. and Tolba, M.T. (2009), "Modelling and analysis of two-way composite slabs", *J. Constr. Steel Res.*, **65**(5), 1236-1248.
- Abdullah, R. and Easterling, S.W. (2009), "New evaluation and modeling procedure for horizontal shear bond in composite slabs", *J. Constr. Steel Res.*, **65**(4), 891-899.
- Airumyan, E., Belyaev, V., and Romyancev, I. (1990), "Efficient embossment for corrugated steel sheeting", *IABSE Symposium on Mixed Structures Including New Materials*, Brussels, Belgium, September.
- Al-deen, S., Ranzi, G. and Vrcelj, Z. (2011a), "Full-scale long-term experiments of simply-supported composite beams with solid slabs", *J. Constr. Steel Res.*, **67**(3), 308-321.
- Al-deen, S., Ranzi, G. and Vrcelj, Z. (2011b), "Full-scale long-term and ultimate experiments of simply-supported composite beams with steel deck", *J. Constr. Steel Res.*, **67**(10), 1658-1676.
- Al-Deen, S., Ranzi, G. and Vrcelj, Z. (2012), "Long-term experiments of composite beams and connections", *Mag. Concrete Res.*, **64**(9), 849-861.
- Alsamsam, I. (1991), "Serviceability criteria for composite floor systems", Ph.D. Thesis, The University of Minnesota, Minneapolis, MN, USA.
- AS3600 (2009), AS3600-2009 Concrete Structures, Standards Australia.
- Bazant, Z.P. (1972), "Prediction of concrete creep effects using age-adjusted effective modulus method", *ACI J.*, **69**(4), 212-217.
- Bazant, Z.P. and Oh, B.H. (1984), "Deformation of progressively cracking reinforced concrete beams", *ACI J.*, **81**(3), 268-278.
- Bradford, M.A. (2010), "Generic modelling of composite steel-concrete slabs subjected to shrinkage, creep and thermal strains including partial interaction", *Eng. Struct.*, **32**(5), 1459-1465.
- Bradford, M.A. and Gilbert, R.I. (1991), "Time-dependent behaviour of simply-supported steel-concrete composite beams", *Mag. Concrete Res.*, **43**(157), 265-274.
- CEB (1984), CEB Design manual on structural effects of time-dependent behaviour of concrete, Georgi Publishing, Saint-Saphorin, Switzerland.
- Chen, S. and Shi, X. (2011), "Shear bond mechanism of composite slabs — A universal FE approach", *J. Constr. Steel Res.*, **67**(10), 1475-1484.
- Chen, S., Shi, X. and Qiu, Z. (2011), "Shear bond failure in composite slabs— a detailed experimental study", *Steel Compos. Struct., Int. J.*, **11**(3), 233-250.
- Crisinel, M. and Marimon, F. (2004), "A new simplified method for the design of composite slabs", *J. Constr. Steel Res.*, **60**(3-5), 481-491.
- Daniels, B.J. and Crisinel, M. (1993), "Composite slab behavior and strength analysis. Part II: Comparisons with test results and parametric analysis", *J. Struct. Eng.*, **119**(1), 36-49.
- Easterling, W.S. and Young, C.S. (1992), "Strength of composite slabs", *J. Struct. Eng.*, **118**(9), 2370-2389.
- Fan, J., Nie, J., Li, Q. and Wang, H. (2010), "Long-term behavior of composite beams under positive and

- negative bending. I: Experimental study”, *J. Struct. Eng.*, **136**(7), 849-857.
- Gholamhoseini, A., Gilbert, R.I., Bradford, M.A. and Chang, Z.T. (2012), “Long-term deformation of composite concrete slabs”, *Concrete in Australia*, **38**(8), 25-32.
- Gilbert, R.I. and Ranzi, G. (2011), *Time-Dependent Behaviour of Concrete Structures*, Spon Press, London, UK.
- Gilbert, R.I., Bradford, M.A., Gholamhoseini, A. and Chang, Z.T. (2012), “Effects of shrinkage on the long-term stresses and deformations of composite concrete slabs”, *Eng. Struct.*, **40**, 9-19.
- Jeong, Y.-J., Kim, H.-Y. and Kim, S.-H. (2005), “Partial-interaction analysis with push-out tests”, *J. Constr. Steel Res.*, **61**(9), 1318-1331.
- Johnson, R.P. (1987), “Shrinkage induced curvature in composite beams with a cracked concrete flange”, *Struct. Eng.*, **65B**(4), 72-76.
- Kim, H.-Y. and Jeong, Y.-J. (2010), “Ultimate strength of a steel–concrete composite bridge deck slab with profiled sheeting”, *Eng. Struct.*, **32**(2), 534-546.
- Lopes, E. and Simões, R. (2008), “Experimental and analytical behaviour of composite slabs”, *Steel Compos. Struct., Int. J.*, **8**(5), 361-388.
- Marimuthu, V., Seetharaman, S., Arul Jayachandran, S., Chellappan, A., Bandyopadhyay, T.K. and Dutta, D. (2007), “Experimental studies on composite deck slabs to determine the shear-bond characteristic values of the embossed profiled sheet”, *J. Constr. Steel Res.*, **63**(6), 791-803.
- Onesteel (2012), <http://www.onesteel.com/>
- Patrick, M. and Bridge, R.Q. (1994), “Partial shear connection design of composite slabs”, *Eng. Struct.*, **16**(5), 348-362.
- Patrick, M. and Poh, K.W. (1990), “Controlled test for composite slab design parameters”, *LABSE Symposium on Mixed Structures Including New Materials*, Brussels, Belgium, September.
- Porter, M.L. (1985), “Analysis of two-way acting composite”, *J. Struct. Eng.*, **111**(1), 1-18.
- Porter, M.L. and Ekberg Jr., C.E. (1977), “Behavior of steel-deck-reinforced slabs”, *J. Struct. Div., ASCE*, **103**(3), 663-677.
- Ranzi, G. and Vrcelj, Z. (2009), “Closed form solutions for the long-term analysis of composite steel-concrete members subjected to non-uniform shrinkage distributions”, *Proceedings of the Sixth International Conference on Advances in Steel Structures*, Hong Kong, December.
- Ranzi, G., Al-deen, S., Ambrogi, L. and Uy, B. (2013a), “Long-term behaviour of simply-supported post-tensioned composite slabs”, *J. Constr. Steel Res.*, **88**, 172-180.
- Ranzi, G., Leoni, G. and Zandonini, R. (2013b), “State of the art on the time-dependent behaviour of composite steel-concrete structures”, *J. Constr. Steel Res.*, **80**, 252-263.
- Roll, F. (1971), “Effects of differential shrinkage and creep on a composite steel-concrete structure”, *ACI Special Publication*, **SP-27**(8), 187-214.
- Seres, N. and Dunai, L. (2011), “Experimental and numerical studies on concrete encased embossments of steel strips under shear action for composite slabs with profiled steel decking”, *Steel Compos. Struct., Int. J.*, **11**(1), 39-58.
- Stark, J.W.B. and Brekelmans, J.W.P.M. (1990), “Plastic design of continuous composite slabs”, *J. Constr. Steel Res.*, **15**(1-2), 23-47.
- Stramit (2012), www.stramit.com.au
- Uy, B. (1997), “Long-term service load behaviour of simply-supported profiled composite slabs”, *Structures and Buildings, Proceedings of the Institution of Civil Engineers*, **122**(2), 193-208.
- Veljković, M. (1996), “Behaviour and resistance of composite slabs”, Ph.D. Theiss, Lulea University of Technology, Lulea, Sweden.
- Veljković, M. (1998), “Influence of load arrangement on composite slab behaviour and recommendations for design”, *J. Constr. Steel Res.*, **45**(2), 149-178.
- Wright, H.D., Vitek, J.L. and Rakib, S.N. (1992), “Long-term creep and shrinkage in composite beams with partial connection”, *ICE Proceedings, Structures and Buildings*, **94**(2), 187-195.